Dynamics of the frustrated anisotropic $J_1 - J_2$ chain

H.-J. Mikeska

Institut für Theoretische Physik, Universität Hannover, 30167 Hannover, Germany

December 2015

Model

$$H = J_1 \sum \{(S_n^x S_{n+1}^x + S_n^y S_{n+1}^y) + \Delta S_n^z S_{n+1}^z\}$$
$$+ J_2 \sum \{(S_n^x S_{n+2}^x + S_n^y S_{n+2}^y) + \Delta S_n^z S_{n+2}^z\} \quad (1)$$

N spins 1/2, ferromagnetic nearest neighbour coupling $J_1 < 0$ and antiferromagnetic next nearest neighbour coupling J_2. Lanczos diagonalization for chains with $N = 24, 20, 16, 12$ spins, the unit of energy is fixed by choosing $J_2 = +1$.

Aim of the work

Calculate and discuss the dynamics (lowest excitations) in the full range of the phase space spanned by $0 \leq \Delta \leq 1$ and $-J_1$ going from 0 to very large values. Identify the various phases in this regime and compare to the DMRG work of Furusaki et al.

Points and lines with exact results in the $\Delta - J_1$ phase diagram:

- line $J_1 = 0$: two decoupled anisotropic HAFs with $N/2$ spins (i.e. doubled lattice constant, $2a$), where exact results on the infinite system are available from Bethe ansatz.
- $J_1 = 0, \Delta = 0$: $S = 1/2$ $xy-$chain, where the exact results are available after transformation to fermions (LSM). In particular, exact results are available for arbitrary finite size.
- $J_1 = -2, \Delta = 0$: Majumdar-Ghosh point, where the ground state is known to be a product state of ferromagnetic dimers with $S_{tot}^z = 0$. The excitations are solitons with a gap. This point is the ferromagnetic version of the Majumdar-Ghosh point originally described for the antiferromagnetic chain with NNN exchange, $J_1, J_2 > 0$.

- $-J_1 = 4, \Delta = 1.0$: At this point the phase transition to the ferromagnetic ground state (which is trivially realized for very large J_1) occurs. Whereas for $\Delta = 1.0$ the ground state has $S_{tot} = 0$ for $-J_1 < 4$ and $S_{tot} = S_{max} = N/2$ for $-J_1 > 4$, for $\Delta < 1.0$ it has $S^z_{tot} = 0$ for all $-J_1$.

- $-J_1 \gg J_2$: the system approaches the limit of an anisotropic ferromagnetic Heisenberg chain (lattice constant a), which is also covered by the Bethe ansatz solution.

Results so far:

- phase diagram $\Delta - -J_1$ in comparison to DMRG results (Furukawa, Sato, Onoda, Furusaki, PRB 86, 094417 (2013)):
  we identify the vector chiral phase by minima $k \neq \pi/2$, a maximum number of 3 minima ($k = p\pi/4, p = 1, 2, 3$) is found at $-J_1 = 3.50, \Delta = 1$ (fig. 13)
  we identify the dimer phase by a gap in the spectrum and, alternatively, by a second degenerate ground state at $k = \pi$ (figs. 17 - 19).
  the line separating the C and IC regimes inside the dimer phase is found in complete agreement with DMRG (20).
  the extent of the dimer regime is underestimated by the approach of looking for degenerate ground states and roughly correct in the approach of looking for a vanishing gap

- type of excitations:
  The transition from the double sine dispersion at small J_1 to the sine ($xy-$) dispersion at large $-J_1$ is nicely seen. The intermediate stages of gapped spectra and modulated spectra can be clearly followed.
  A method describing the modulation in the vector chiral phase has still to be developped.

- Finite size effects:
  extrapolation to $N \to \infty$ from $N = 16$ and $N = 24$ gives reasonable results for small $-J_1$, e.g. the vanishing of the gap is obtained.
  For larger $-J_1$ the $N-$dependence is governed by oscillations and a successful extrapolation should take into account the $N-$dependence of the oscillation period.

Figures of dispersions for some overview:

In these figures excitation spectra are shown for $S^z_{tot} = 1$ (lowest state). The zero of energy is defined as the result obtained for $k = 0, S^z_{tot} = 0$. In the majority of cases this conincides with the ground state for the finite system considered. However, in some cases, the state $k = \pi, S^z_{tot} = 0$ has lower energy, which implies the possibility of negative energies in the dispersion curves.

We use integer numbers p as wave vector units,adapted to the chain with 24 spins, where $k = (2\pi/24)\, p$ with $p = 0...23$. Thus $p = 12$ corresponds to π etc. For general number of spins we use $p = (12/\pi)\, k$ to make direct comparison between two different N possible (p is no more necessarily integer). We only show the first half of the BZ, $p = 0...12$, that of the second half follows from reflection invariance.

Fixed Δ (figs. 1 - 4):

- series of spectra for $\Delta = 0$ and $\Delta = 0.5$, varying J_1 from -0.7 to -2.70.
- series of spectra for $\Delta = 1.0$ (isotropic chain), varying J_1 from 0 to -3.50.

Fixed J_1 (figs. 5 - 13):

- series of spectra for $J_1 = -1.0, -1.8, -2.0$, varying Δ from 0 to 1.
- series of spectra for $J_1 = -2.5, -2.7, -3.3, -3.5$ varying Δ from 0.5 to 1.

Some discussion:

Along lines with fixed Δ the spectrum/dispersion changes from the double sine behaviour at small $-J_1$ to the sine behaviour at large $-J_1$. With the exception maybe of values of Δ close to 1, these two regimes are separated by a regime of dimer type, emerging by continuous deformation from the Majumdar-Ghosh point and characterized by two degenerate ground states at $k = 0, \pi$.

A striking property of the spectra is the emergence of minima different from the minimum at $k = 6$ for small $-J_1$. The most prominent of these is at $k = 7$, others are at $k = 4$ and $k = 9$. With increase of $-J_1$ there is a critical value $-J_1^{c1}$ where the minimum shifts from $k = 6$ to $k = 7$, at some larger $-J_1$ this minimum shifts to $k = 9$ and at a second critical value $-J_1^{c2}$ no minimum is left. The line $-J_1^{c2}(\Delta)$ is identified with the Lifshitz line.

Finite size effects and extent of the dimer phase

Possible ground states are at $k = 0$ and $k = \pi$ and we find that the energy difference between these states oscillates with the parameters, an obvious finite size effect as is seen by comparing different N, fig. 14.

Plotting the dispersion for different values of N, figs. 15,16 we find that the position of the minima for various values of N is not in contradiction to the assumption that a reasonable limit for $N \to \infty$ exists. From fig. 16 we conclude that it may be appropriate to measure k wrt the ground state k for the actual N.

The increase of energy close to $k = \pi$ and also $k = 0$ observed in many of the dispersions is very probably a finite size effect: It is also obtained analytically for the simple af chain $xy-$model, which in the free fermion picture can be solved exactly for finite N. It results from a discontinuity in the occupation of fermion bands and only occurs for the final interval in $k-$space nect to $k = 0, \pi$ and thus disappears in the limit $N \to \infty$.

Energy gap and dispersion: When the system enters the dimerized regime, an energy gap opens up at both $k = 0, 12(\equiv 0, \pi)$. This is difficult to see numerically in the finite system since the second lowest states have to be considered. Qualitatively, a $1/N$ extrapolation for $k = 12$ in the regime of small J_1 leads to the expected result 'no gap' as well as in the regime of intermediate $-J_1$ and Δ sufficeintly different from 1 to the expected result: 'finite (dimer) gap'.

Over a finite range of $\Delta-$values (dimer regime) the lowest $k = 12$ state becomes degenerate with the lowest $k = 0$ state (zero energy, taken as zero of energy), the existence of these two degenerate ground states is the signature of the dimerized regime. The degeneracy is seen in a corresponding manner already for both $N = 24$ and for $N = 16$ (figs. 17 - 19) which illustrates how the correlation length drops (well in the dimerized regime, even $N = 16$ is sufficient to produce the degeneracy). An estimate of the extent of the degenerate ground states can serve as an estimate of the extent of the dimerized regimed and was used to obtain the lines shown in fig. 20.

Another characteristic of the dimerized regime is the solitonlike dispersion, obtained by a hopping of the dimer excitation from one dimer to the next one. This can be compared to the analytical soliton dispersion. A characteric of the emerging soliton dispersion is that the energy of the $k = \pi/2$ state starts to deviate from 0, actually it grows linearly.

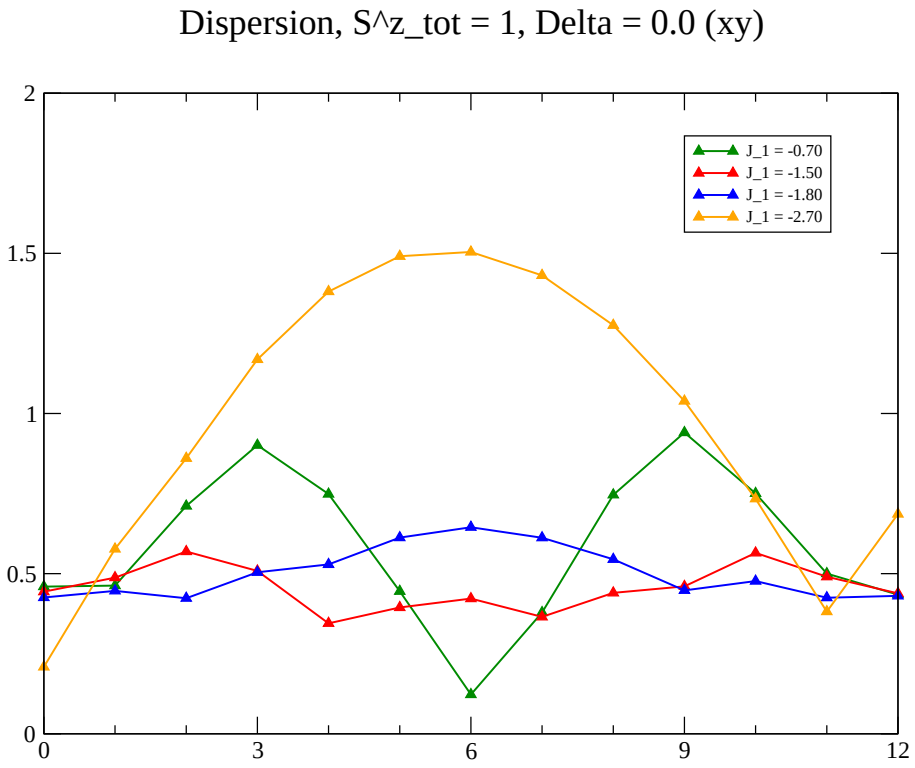

FIG. 1: $S^z_{tot} = 1$ spectra for $N = 24,\ \Delta = 0.00$ and $J_1 = -0.70... - 2.70$.

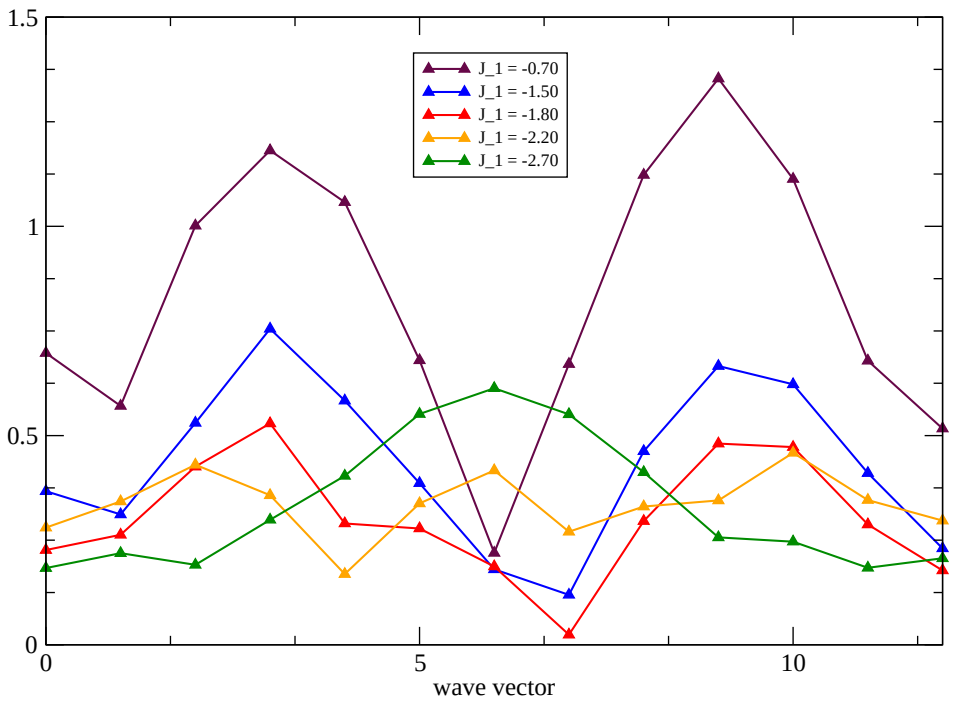

FIG. 2: $S^z_{tot} = 1$ spectra for $N = 24,\ \Delta = 0.50$ and $J_1 = -0.70... - 2.70$.

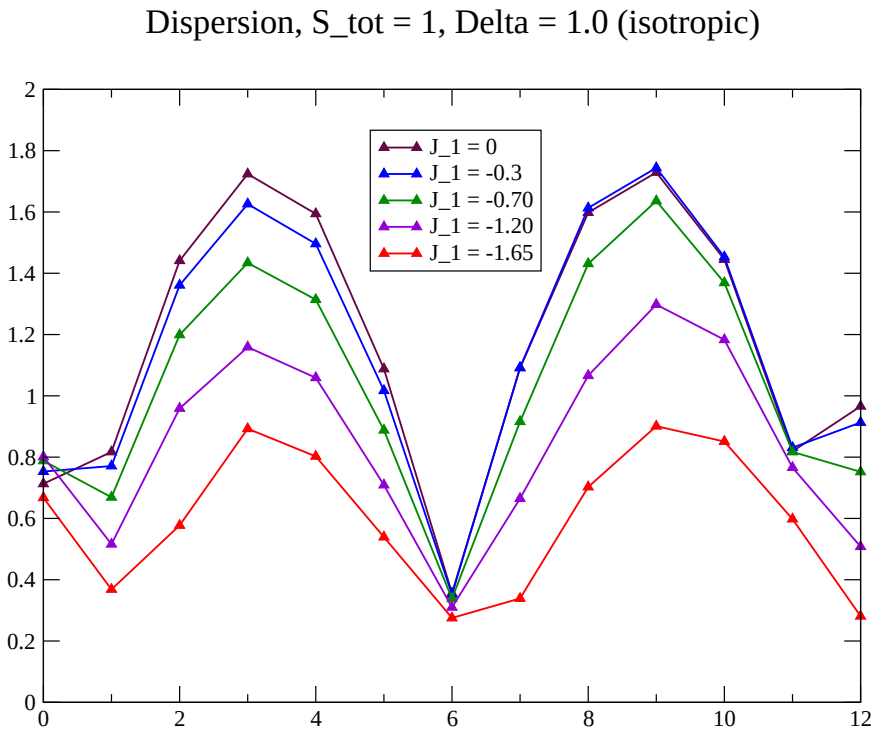

FIG. 3: $S^z_{tot} = 1$ spectra for $N = 24,\ \Delta = 1.00$ and $J_1 = -0... - 1.65$.

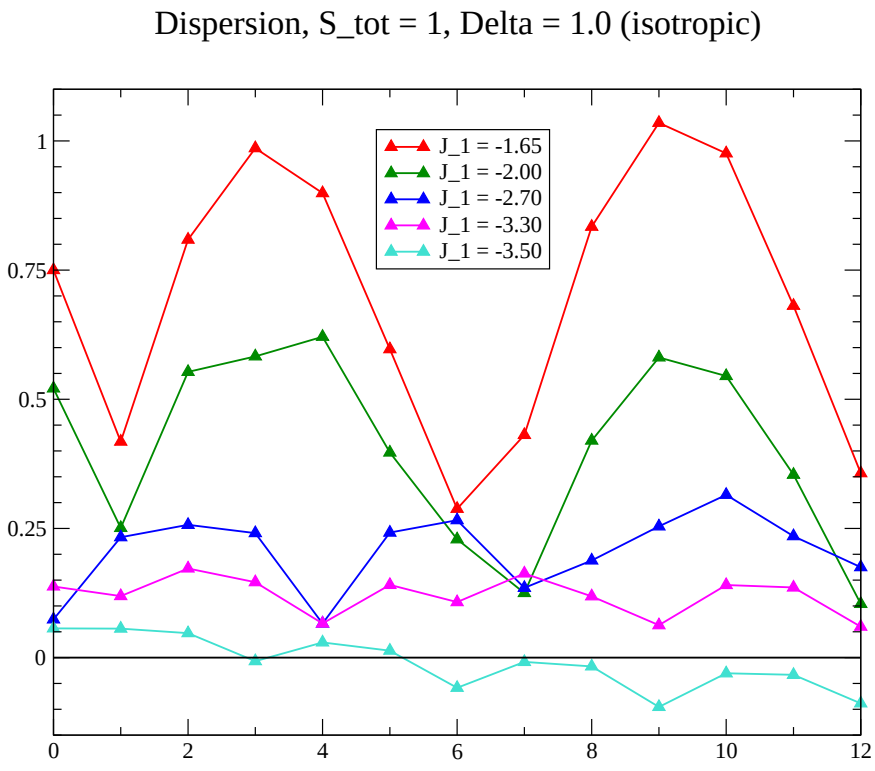

FIG. 4: $S^z_{tot} = 1$ spectra for $N = 24,\ \Delta = 1.00$ and $J_1 = -1.65... - 3.50$.

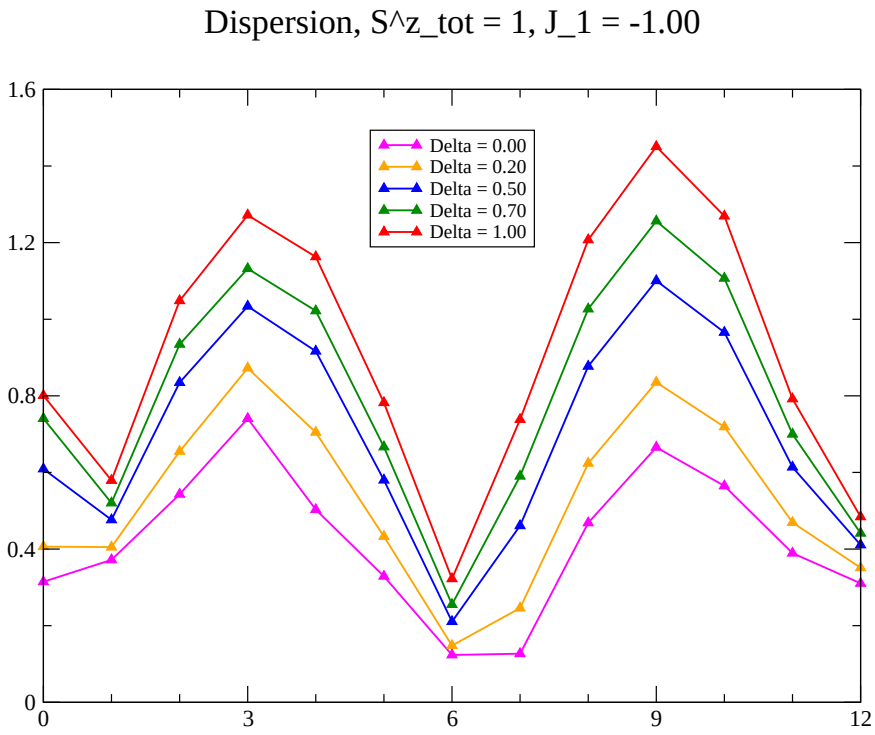

FIG. 5: $S^z_{tot} = 1$ spectra for $N = 24, J_1 = -1.0$ and $\Delta = 0...1$.

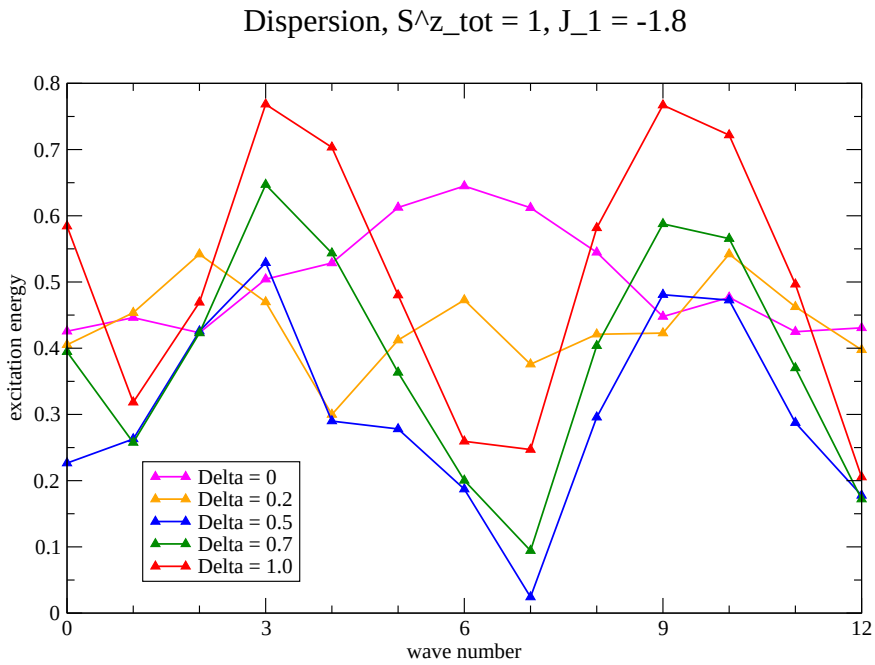

FIG. 6: $S^z_{tot} = 1$ spectra for $N = 24, J_1 = -1.8$ and $\Delta = 0...0.7$.

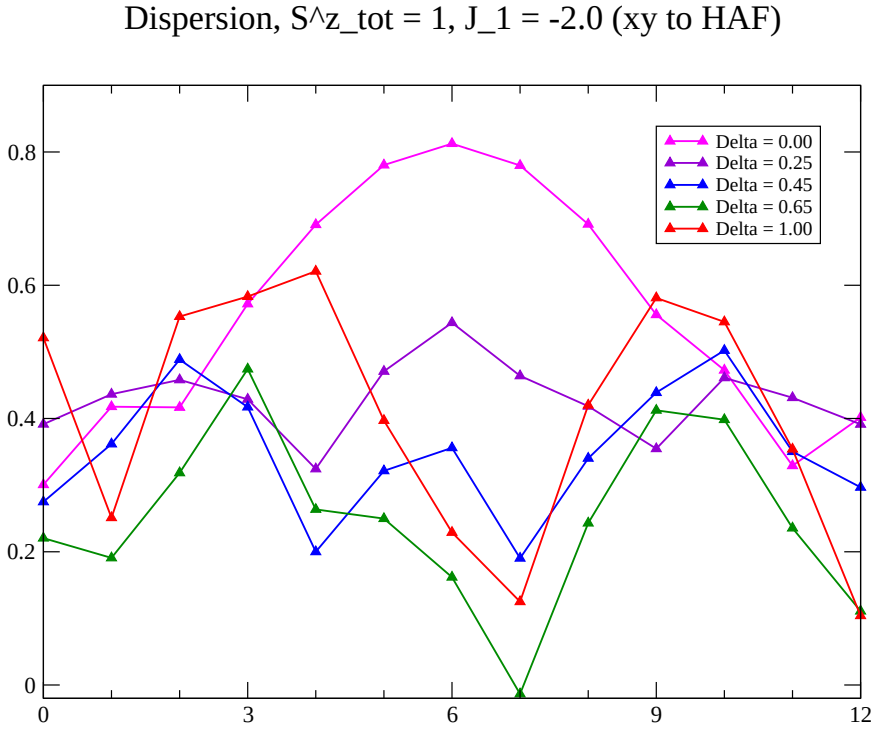

FIG. 7: $S^z_{tot} = 1$ spectra for $N = 24, J_1 = -2.0$ and $\Delta = 0...1$.

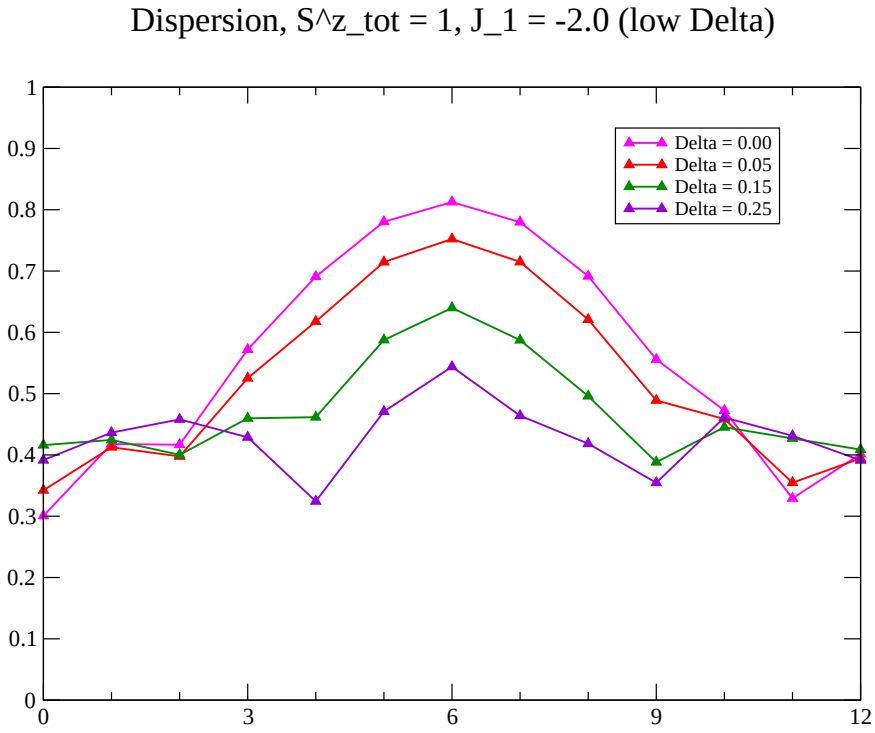

FIG. 8: $S^z_{tot} = 1$ spectra for $N = 24, J_1 = -2.0$ and $\Delta = 0...0.25$.

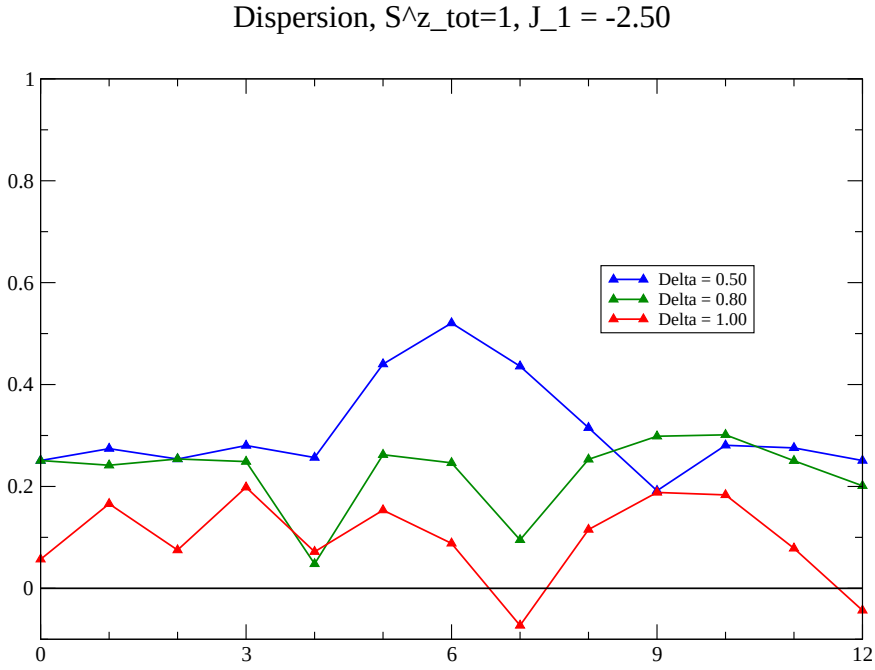

FIG. 9: $S^z_{tot} = 1$ spectra for $N = 24, J_1 = -2.5$ and $\Delta = 0...1$.

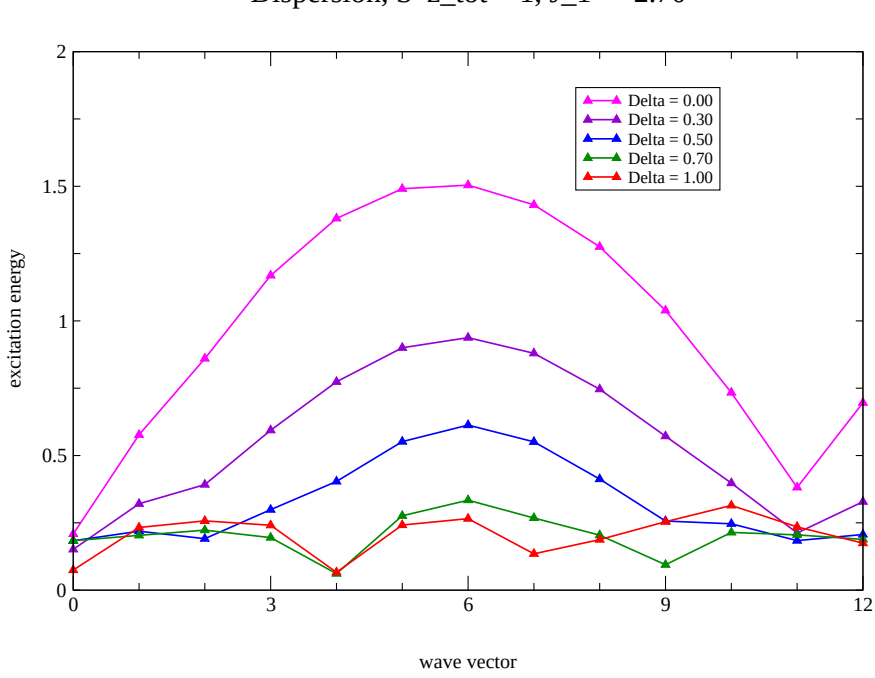

FIG. 10: $S^z_{tot} = 1$ spectra for $N = 24, J_1 = -2.7$ and $\Delta = 0...1$.

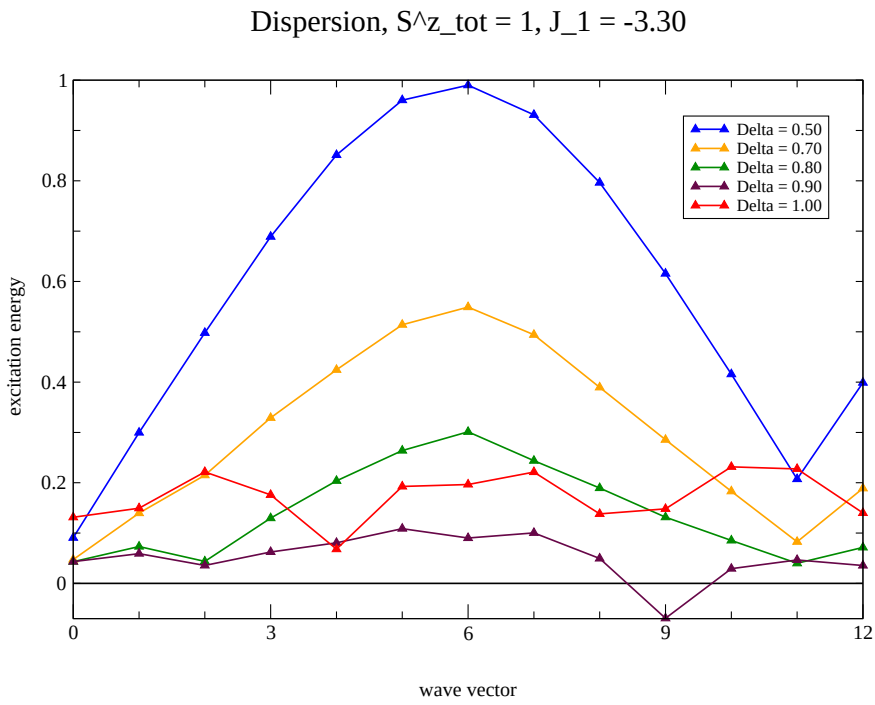

FIG. 11: $S^z_{tot} = 1$ spectra for $N = 24, J_1 = -3.3$ and $\Delta = 0.5...1$.

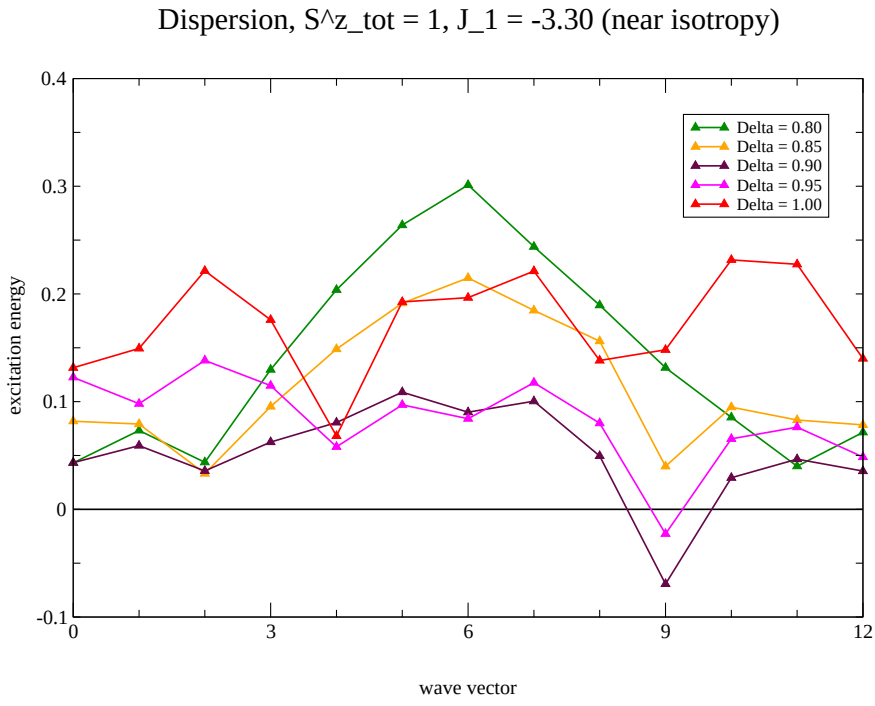

FIG. 12: $S^z_{tot} = 1$ spectra for $N = 24, J_1 = -3.3$ and $\Delta = 0.8...1$ (approach to isotropy).

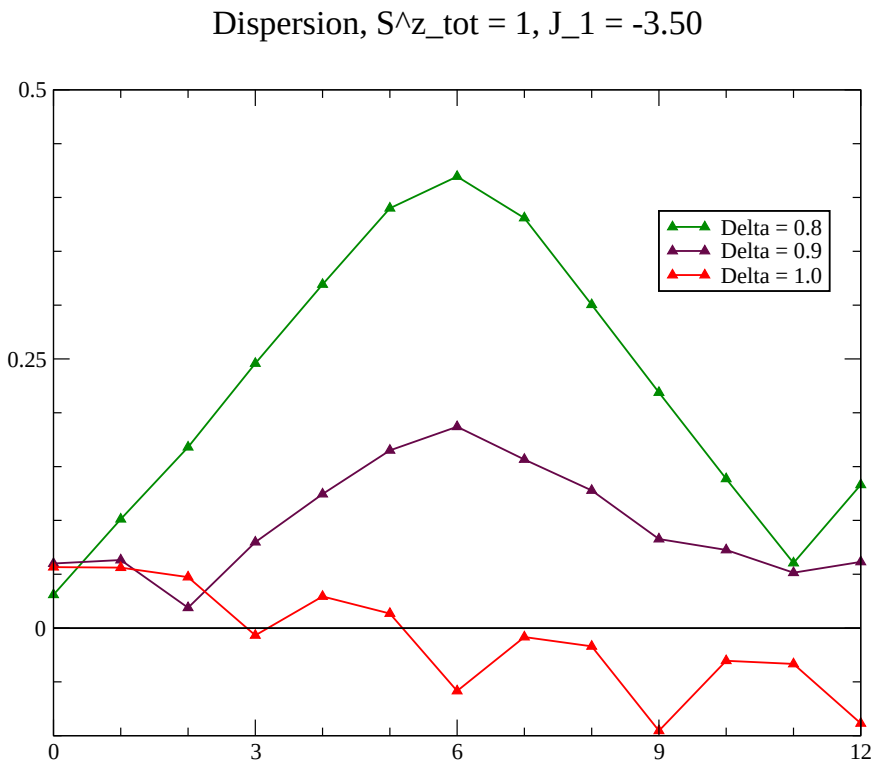

FIG. 13: $S^z_{tot} = 1$ spectra for $N = 24, J_1 = -3.5$ and $\Delta = 0.8, 0.9, 1.0$. For $J_1 = -3.5$ and $k = \pi$ energies of both lowest and first excited state are below the lowest energy for $k = 0$.

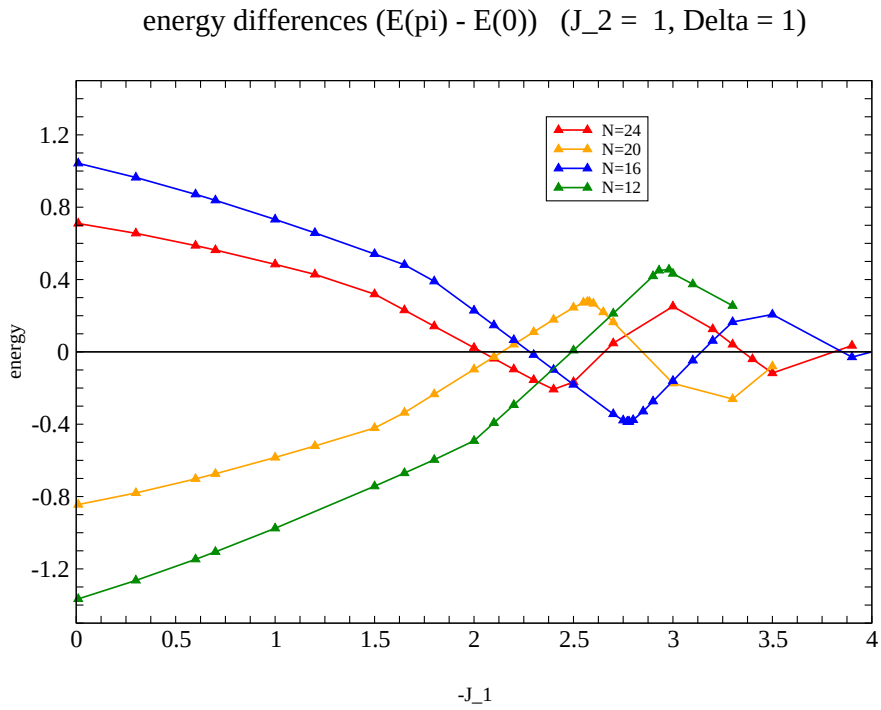

FIG. 14: $N-$dependence of difference of energies at $k = \pi$ and $k = 0$ for $S_{tot} = 1$: $N = 24, 20, 16$ and 12, $J_1 = -3.00$ and $\Delta = 1.00$.

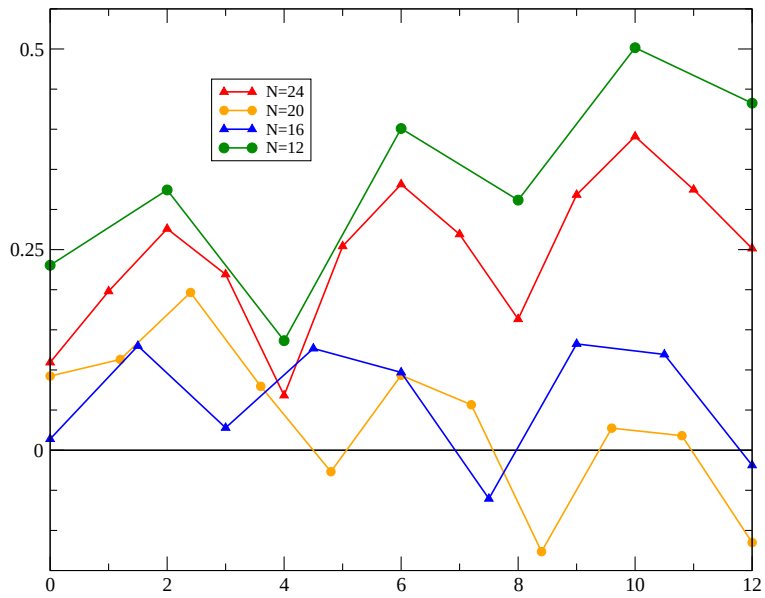

FIG. 15: $S^z_{tot} = 1$ spectra for $N = 24, 20, 16$ and 12, $J_1 = -3.00$ and $\Delta = 1.00$.

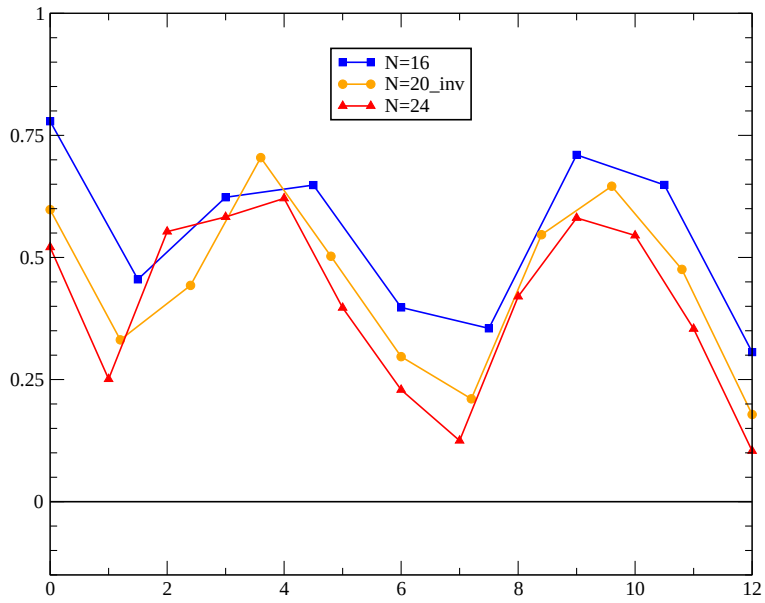

FIG. 16: Spectra for $N = 24, 20$ and 16, $\Delta = 1.00$ and $J_1 = -2.00$. Inverted $k-$range for $N = 20$.

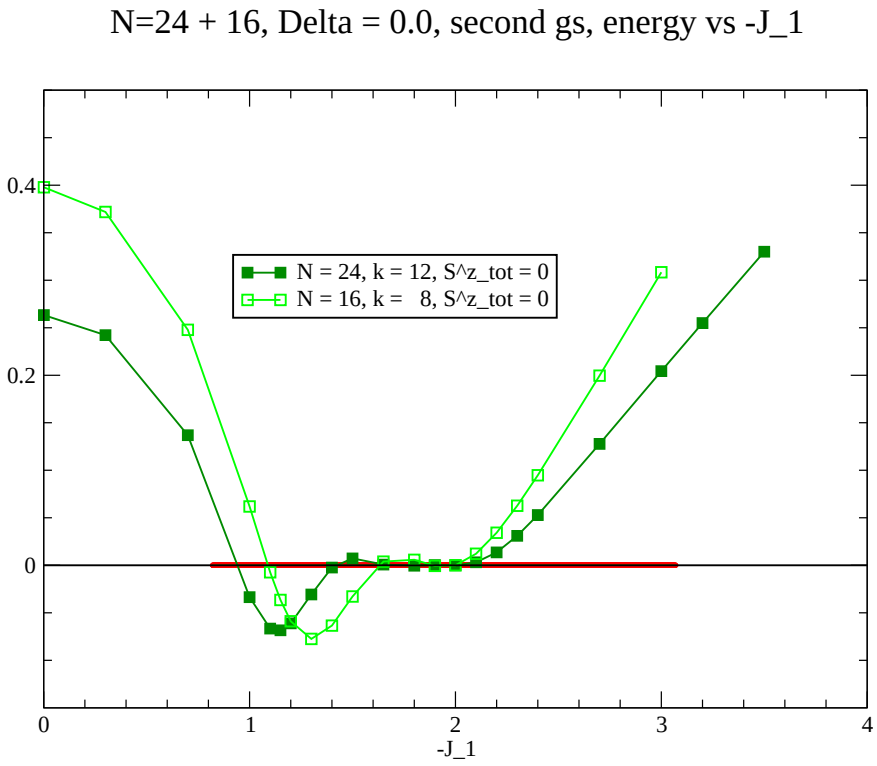

FIG. 17: energy of the possible second ground state at $k = \pi, S^z_{tot} = 0$ for $\Delta = 0$ vs. $-J_1$ for $N = 24$ and $N = 16$. The red part of the $x-$axis indicates the range of the dimer regime from DMRG [Furusaki]

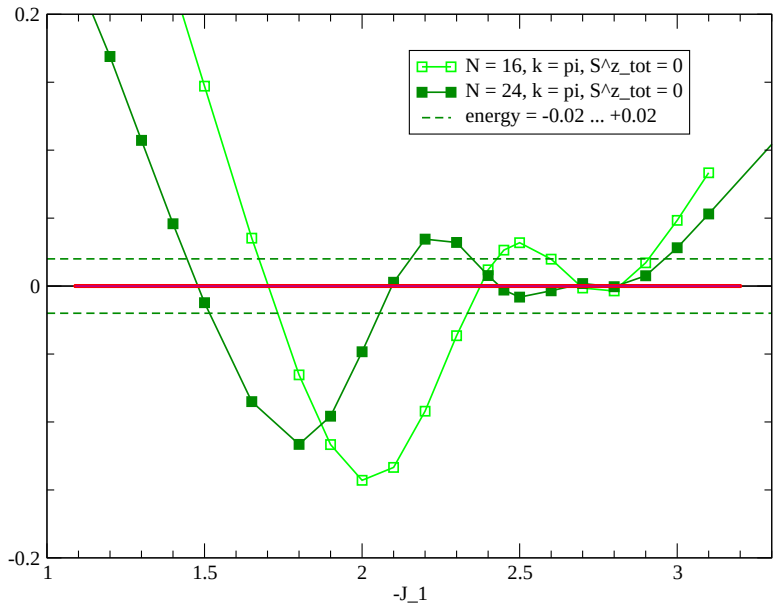

FIG. 18: energy of the possible second ground state at $k = \pi, S^z_{tot} = 0$ for $\Delta = 0.5$ vs. $-J_1$ for $N = 24$ and $N = 16$. The red part of the $x-$axis indicates the range of the dimer regime from DMRG

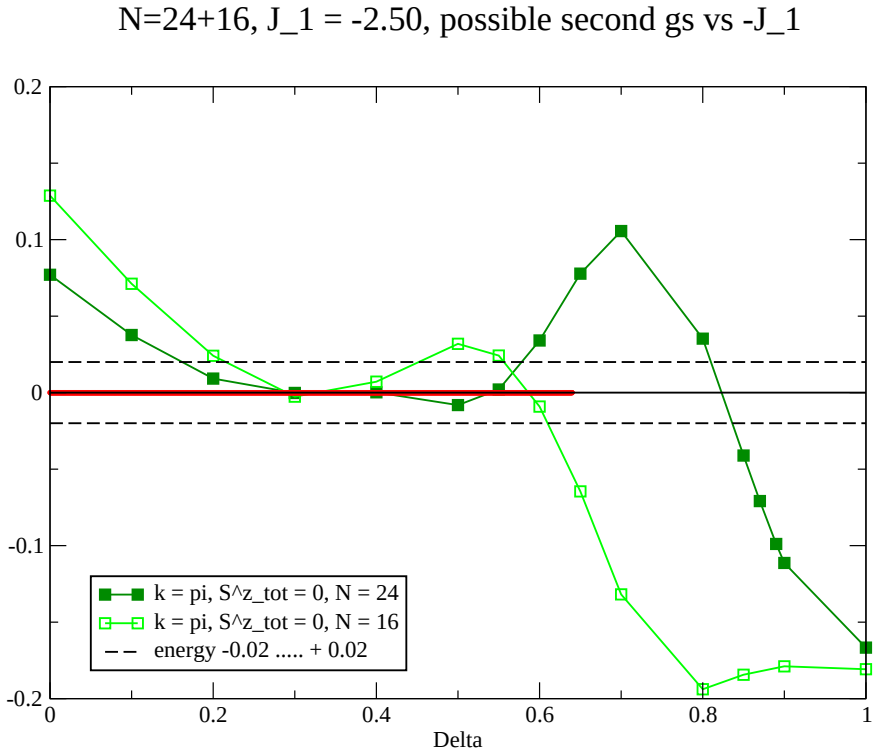

FIG. 19: energy of the possible second ground state at $k = \pi, S^z_{tot} = 0$ for $J_1 = -2.5$ vs. Δ for $N = 24$ and $N = 16$. The red part of the $x-$axis indicates the range of the dimer regime from DMRG

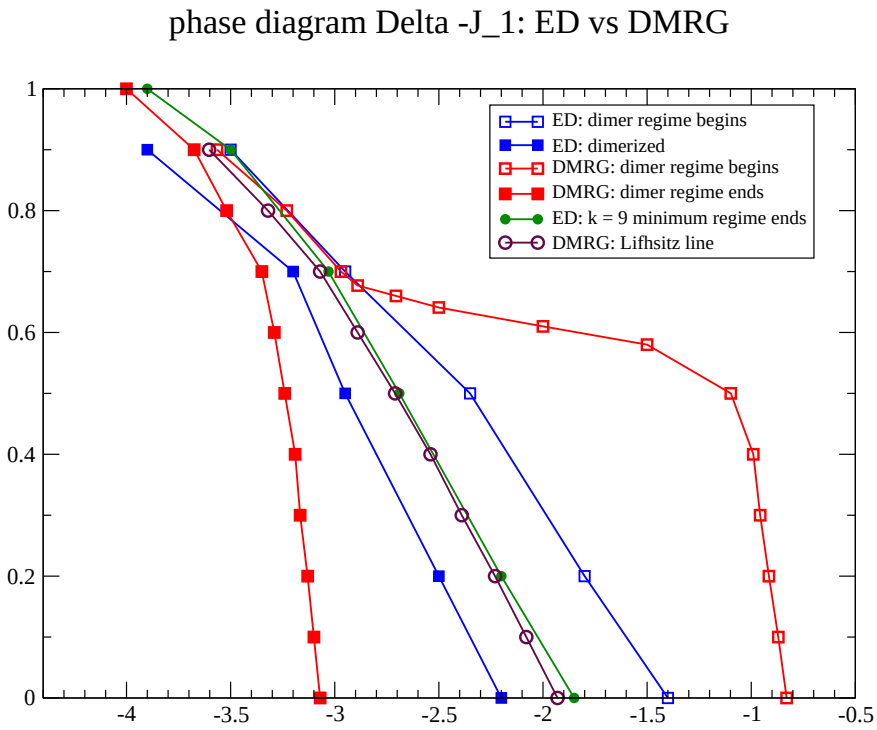

FIG. 20: Phase diagram Δ vs J_1: comparison of DMRG results to ED resuls, $N = 24$.

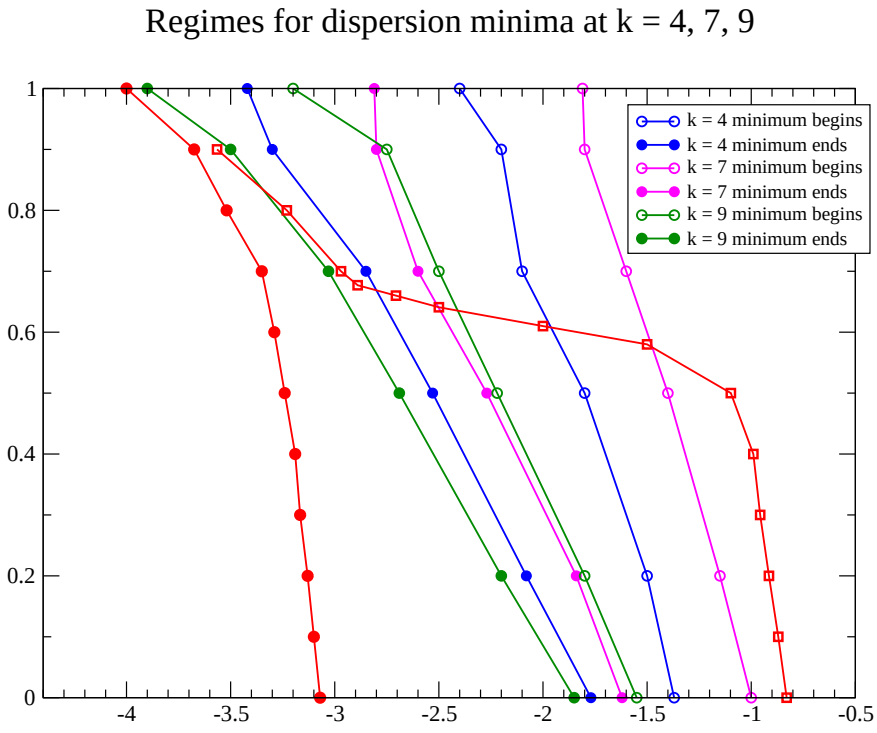

FIG. 21: Phase diagram Δ vs J_1: extent of regimes for dispersion minima in ED for $N = 24$.